NEOPLASIA
www.neoplasia.com

Volume 000 Number xxx xxx 2020 pp. 1–10

Original Research

Hypoxia theranostics of a human prostate cancer xenograft and the resulting effects on the tumor microenvironment☆,☆☆

Balaji Krishnamachary[a,*]; Yelena Mironchik[a]; Desmond Jacob[a]; Eibhlin Goggins[a]; Samata Kakkad[a]; Francis Ofori[a]; Louis Dore-Savard[a]; Santosh Kumar Bharti[a]; Flonne Wildes[a]; Marie-France Penet[a,b]; Margaret E Black[d]; Zaver M Bhujwalla[a,b,c,*]

[a] Division of Cancer Imaging Research, The Russell H. Morgan Department of Radiology and Radiological Science, The Johns Hopkins University School of Medicine, Baltimore, MD
[b] Sidney Kimmel Comprehensive Cancer Center, The Johns Hopkins University School of Medicine, Baltimore, MD
[c] Radiation Oncology and Molecular Radiation Sciences, The Johns Hopkins University School of Medicine, Baltimore, MD
[d] School of Molecular Biosciences, Washington State University, Pullman, WA

Abstract

Hypoxia is frequently observed in human prostate cancer, and is associated with chemoresistance, radioresistance, metastasis, and castrate-resistance. Our purpose in these studies was to perform hypoxia theranostics by combining *in vivo* hypoxia imaging and hypoxic cancer cell targeting in a human prostate cancer xenograft. This was achieved by engineering PC3 human prostate cancer cells to express luciferase as well as a prodrug enzyme, yeast cytosine deaminase, under control of hypoxic response elements (HREs). Cancer cells display an adaptive response to hypoxia through the activation of several genes mediated by the binding of hypoxia inducible factors (HIFs) to HRE in the promoter region of target gene that results in their increased transcription. HIFs promote key steps in tumorigenesis, including angiogenesis, metabolism, proliferation, metastasis, and differentiation. HRE-driven luciferase expression allowed us to detect hypoxia *in vivo* to time the administration of the nontoxic prodrug 5-fluorocytosine that was converted by yeast cytosine deaminase, expressed under HRE regulation, to the chemotherapy agent 5-fluorouracil to target hypoxic cells. Conversion of 5-fluorocytosine to 5-fluorouracil was detected *in vivo* by ^{19}F magnetic resonance spectroscopy. Morphological and immunohistochemical staining and molecular analyses were performed to characterize tumor microenvironment changes in cancer-associated fibroblasts, cell viability, collagen 1 fiber patterns, and HIF-1α. These studies expand our understanding of the effects of eliminating hypoxic cancer cells on the tumor microenvironment and in reducing stromal cell populations such as cancer-associated fibroblasts.

Neoplasia (2020) 000, 1–10

Keywords: Hypoxia, Prodrug enzyme, Imaging, Prostate cancer, Cancer-associated fibroblasts, Collagen 1 fibers

Introduction

Hypoxic environments frequently exist in solid tumors and result in resistance to therapy and the evolution of a more lethal phenotype. The

* Corresponding authors. Department of Radiology, The Johns Hopkins University School of Medicine, 720 Rutland Avenue, #208C Traylor Building, Baltimore, MD 21235.
E-mail addresses: bkrishn1@jhmi.edu (B. Krishnamachary), zbhujwa1@jhmi.edu (Z.M. Bhujwalla).

☆ Declaration of competing interest: None.

☆☆ Abbreviations: 5-FC, 5-fluorocytosine; 5-FU, 5-fluorouracil; BLI, bioluminescence imaging; CAFs, cancer-associated fibroblasts; CD, cytosine deaminase; Col1, collagen 1; ECM, extracellular matrix; HIF-1α, hypoxia inducible factor-1α; HRE, hypoxic response element; MRS, magnetic resonance spectroscopy; SHG, second harmonic generation; TME, tumor microenvironment; α-SMA, α smooth muscle actin.

Received 11 August 2020; received in revised form 1 October 2020; accepted 4 October 2020; Available online xxx

https://doi.org/10.1016/j.neo.2020.10.001

evolution of this lethal phenotype is mediated to a large extent by hypoxia inducible factors (HIFs) binding to hypoxia response elements (HREs) and inducing the transcriptional activation of several target genes [1]. HIF is a heterodimeric basic helix-loop-helix PAS (Per-ARNT-Sim) domain containing transcription factor that consists of a constitutively expressed β-subunit (HIF-β/ARNT) and one of 3 oxygen-regulated α-subunits, HIF-1α, HIF-2α and HIF-3α. The α-subunits are constitutively transcribed and translated, but are regulated at the protein level by oxygen-dependent hydroxylation of specific prolyl residues that target them for ubiquitination by the von Hippel-Lindau protein (pVHL)-E3 ubiquitin ligase complex, and for subsequent proteasomal degradation under normoxia [1]. In addition, oxygen dependent asparagyl hydroxylation in the C-terminal transactivation domain of the HIF-α subunits modulates their transcriptional activity.

HIFs play an integral role in angiogenesis, metabolism, proliferation, metastasis, and differentiation [1]. HIF-α subunits may also be subject to modulation in the absence of hypoxia by growth factor signaling pathways. HIF-1α and HIF-2α expression is increased in many human tumors, including bladder, breast, colon, glial, hepatocellular, ovarian, pancreatic, prostate, and renal tumors [1]. HIF-1α expression is frequently observed with immunostaining in human prostate cancer specimens [2]. HIF-1α overexpression is also observed in the absence of hypoxia, even though VHL mutations are rare in prostate cancer [2]. Irrespective of the causes of HIF-1α expression, its role in prostate cancer chemoresistance, radioresistance, metastasis, castrate-resistance [2], and most recently its association with stem-like prostate cancer cells [3–5] is clearly emerging. Stem-like cancer cells are increasingly being identified as populations in prostate cancer that contribute to metastasis and chemo-/radioresistance [6]. In prostate cancer, HIF-1α expression and hypoxia have also been closely associated with prostate stem cell markers such as NANOG and OCT4 [3].

Stromal cells play a critical role in tumor progression [7,8]. Among these, cancer-associated fibroblasts (CAFs) significantly influence the proliferation, invasion, and metastasis of cancer cells [8,9], including prostate cancer [8,10–13]. CAFs are a major source of collagen 1 (Col1) fibers in the tumor stroma, and contribute to the reactive desmoplastic tumor stroma and the high density and stiffness of the tumor ECM [14]. We previously identified structural and functional differences between a metastasis permissive and metastasis restrictive prostate cancer extracellular matrix (ECM) that included significant differences in Col1 fiber patterns, and the number of CAFs [15]. Understanding the relationship between eliminating hypoxic cancer cells and the presence of CAFs in tumors can provide new insights into factors that play a role in attracting CAFs in tumors.

HRE-driven imaging reporter systems can be used to report on HIF expression. The binding of HIF to the HRE drives the expression of an imaging reporter such as green fluorescence protein (GFP) or a bioluminescence inducing enzyme such as luciferase [16]. Cells that stably express such constructs provide valuable systems to noninvasively interrogate the temporal and spatial evolution of hypoxia and HIF-1α expression in tumors.

The prodrug enzyme cytosine deaminase (CD), found in bacteria and yeast, converts the nontoxic prodrug 5-fluorocytosine (5-FC) to the anticancer drug 5-fluorouracil (5-FU) that is widely used in the treatment of a range of cancers [17]. Although both yeast and bacterial CD generate 5-FU from 5-FC, the enzymes differ in terms of stability and efficacy [18,19]. Controlling the expression of CD by HRE in cells that also report on HIF-1α expression with luciferase expression, provides a strategy to generate 5-FU directly within cells only when HIF-1α is present, for a theranostic approach to detect and target hypoxic cancer cells.

Here, for the first time, we engineered the PC3 human prostate cancer cell line to carry HRE driven expression of luciferase that reported on temporal and spatial HIF-1α expression with bioluminescence-imaging (BLI). The same cell line also carried HRE-driven expression of yeast yCD to convert 5-FC to 5-FU under hypoxic conditions. Tumors derived from these cells allowed us to perform hypoxia theranostics. Hypoxia was detected *in vivo* with BLI, and the conversion of 5-FC to 5-FU was detected in tumors *in vivo* by ^{19}F magnetic resonance spectroscopy (MRS). Administration of 5-FC, once hypoxia was detected with BLI, allowed us to identify, with immunohistochemistry (IHC), the effect of eliminating hypoxic cells with 5-FU on tumor microenvironment (TME) changes in CAFs, tumor volume and cell viability, as well changes in HIF-1α. Because we detected changes in CAFs that are a major source of Col1 fibers in tumors, second harmonic generation (SHG) microscopy was used to detect changes in Col1 fiber patterns in treated tumors. These studies expand our understanding of the impact of eliminating hypoxic populations on the TME.

Methods

Construction of HRE regulated luciferase and yCD plasmids

A plasmid containing 5 tandem repeats of hypoxia response elements (5X-HRE) with the oxygen dependent degradation domain (ODD), with a nuclear localization signal (NLS) kindly provided by Dr. Hiroshi Harada (Kyoto University) [20], was digested with a restriction enzyme to transfer the 5X-HRE-NLS-ODD-luciferase (HRE_LUC) cassette to the lentiviral vector pMA3211 (Addgene) as shown in Figure 1A. A thermostabilized yCD mutant (yCDtriple) gene in a pET vector was kindly provided by Dr. Margaret E. Black [21]. The yCD gene was amplified, and subcloned downstream of an NLS sequence into a shuttle vector with a 5XHRE-ODD-NLS cassette. Upon sequence verification, the 5XHRE-ODD-NLS-yCD cassette (HRE_yCD) was isolated by restriction digestion and sub cloned into a lentiviral vector as shown in Figure 1B.

Generation and validation of PC3 sub-lines

PC3 human prostate cancer cells were purchased from ATCC (Manassas, VA). Virions expressing either HRE_LUC or HRE_yCD were generated by transfecting 293T cells with a lentivirus vector (HRE_LUC or HRE_yCD), a packaging vector (ΔR8.2) and an envelope vector (pCMV-VSVG), and grown in the presence of 1% fetal bovine serum (FBS) containing DMEM media (SIGMA, St. Louis, MO). Supernatant containing virions was added to PC3 cells to establish cells expressing HRE_LUC. PC3_HRE_LUC cells were treated with 1 µg/mL puromycin to select a high HRE_LUC expressing population. To generate a PC3 subline expressing both HRE_LUC and HRE_yCD (PC3_HRE_LUC_yCD), HRE_yCD expressing virions were added to PC3_HRE_LUC cells. Transduction was performed multiple times to ensure maximum expression of the transgenes. The HRE_LUC transgene expression was first optimized with BLI. These cells were then used to make the HRE_LUC_yCD cells that were optimized by determining enzyme expression under hypoxia by RT-PCR.

Validation of luciferase activity

To quantify luciferase activity, PC3_HRE_LUC and PC3_HRE_LUC_yCD cells were seeded in two 6-well plates, with each cell line seeded in 3 wells. Twenty-four hours later, one 6-well plate was exposed to 1% O_2 in a modular hypoxia chamber (Billups-Rothenberg, Del Mar, CA) that was purged with a gas mixture of 94%N_2, 5% CO_2, and 1% O_2. The other plate was maintained under normoxic conditions. Cells were cultured for an additional 24 h before lysis with a passive lysis buffer (Promega, Madison, WI). Luciferase activity was determined using a multiwell luminescence reader (PerkinElmer) following injecting 10 μL of the luciferase reagent (Luciferase Reporter Assay System, Promega). Three independent experiments were performed. Luciferase expression in response to hypoxia was also detected by BLI as previously described [22]. Briefly, PC3 cells expressing HRE-LUC or HRE-LUC and HRE-yCD were seeded

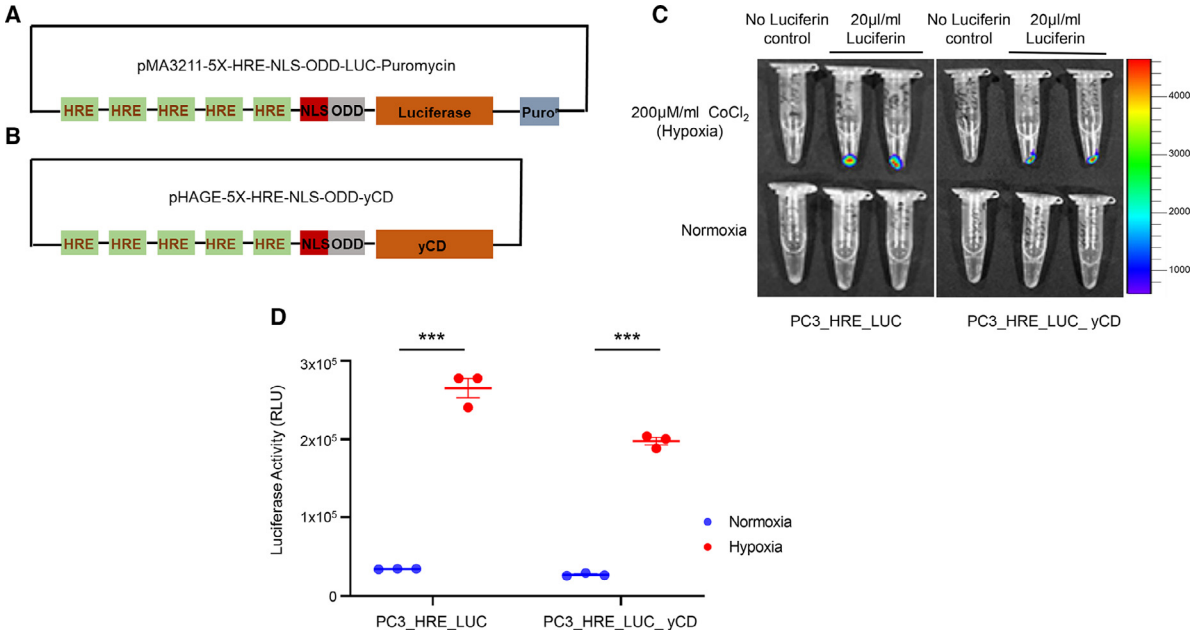

Figure 1. Box and line diagram showing the elements that constitute the lentiviral plasmid expressing, (A) the luciferase gene (A) and (B) the yCD gene, under control of 5 tandem repeats of hypoxia response elements (HREs). The luciferase construct also contains a puromycin resistance cassette that is driven by an SV-40 promoter (not shown in the illustration). (C) Representative BL images showing bioluminescence in PC3 cells expressing different HRE driven constructs in response to the hypoxia mimetic $CoCl_2$. (D) Luciferase assay quantifying the activity of the enzyme in PC3 cells expressing different HRE driven constructs in response to 1% O_2 for 48 h. Values represents Mean ± SEM of 3 independent experiments. $^{***}P < 0.0005$.

at a density of 0.4×10^6 cells in 60 mm petri dishes. Twenty-four hours later, one set of petri dishes was exposed to the hypoxia mimetic cobalt chloride ($CoCl_2$) for 48 h. Cell numbers were determined upon trypsinization. Cells were washed in phosphate buffered saline (PBS) and resuspended in 1 mL of PBS. 20ul of luciferin, (30 mg/mL solution of D-luciferin, P1042, VivoGlo Luciferin, In Vivo Grade, potassium salt, Promega, Madison, WI) was added and cells were briefly spun before detecting bioluminescence on an IVIS Spectrum scanner (Caliper Life Sciences, Hopkinton, MA).

Cell viability

Cell viability of PC3_HRE_LUC and PC3_HRE_LUC_yCD cells in response to hypoxia and the addition of 5-FC was determined using a CCK (cell counting kit) assay (Dojindo Molecular Technologies, Inc., Rockville, MD). Briefly, cells were seeded in 96-well plates at a density of 5000 cells. Each cell line was seeded in at least 16 wells. While one plate was maintained under normoxia in a CO_2 incubator, the second plate was subject to hypoxia in a modular incubator (Billups-Rothenberg, Inc., Del Mar, CA) that was purged with a gas mixture of 94% nitrogen, 5% CO_2, and 1% O_2. Upon preconditioning the cells to either hypoxia or normoxia for 48 h, cells were either treated with 1 mM of 5-FC (SIGMA, St. Louis, Mo) or left untreated as control. Twenty-four hours post 5-FC treatment, 20 µl of CCK-8 reagent was added to each well and incubated in the CO_2 incubator. Formation of yellow colored formazan dye detected colorimetrically at 450 nm indicated dehydrogenase in cells that was directly proportional to the cell number.

Tumor growth and imaging hypoxia in vivo

Tumor xenografts were established by inoculating 2×10^6 PC3_HRE_LUC and PC3_HRE_LUC_yCD cells bilaterally in the flank of five 6 to 8 weeks old male SCID mice. Tumor growth was monitored by measuring tumor volumes with calipers. There were no differences in the growth rate of cells or tumors for the 2 cell lines used. Once tumors were palpable at ~20 mm^3, BLI was performed on an IVIS Spectrum scanner to detect hypoxia following intra peritoneal (i.p) injection of 100 μL of 30 mg/mL D-luciferin solution (Promega, P1042, VivoGlo Luciferin, In Vivo Grade, potassium salt) dissolved in PBS as previously described [23].

All surgical procedures and animal handling were performed in accordance with protocols approved by the Johns Hopkins University Institutional Animal Care and Use Committee, and conformed to the Guide for the Care and Use of Laboratory Animals published by the NIH.

Targeting hypoxic microenvironments

Once hypoxia was detected by BLI in PC3_HRE_LUC and PC3_HRE_LUC_yCD tumors, 5-FC made up in a 15 mg/mL PBS solution was administered at a dose of 250 mg/kg through the tail vein (200 μL) and i.p (750 μL). Four days later, tumor volumes were measured and BLI performed to assess changes in tumor hypoxia followed by a second dose of 5-FC. A third dose, after tumor volume measurements and BLI, was administered 3 days after the second injection, with a final dose administered, after tumor volume measurements and BLI, 4 days after the third dose. Final tumor volume measurements and BLI were performed 7 days after the final dose, after which mice were euthanized and the tumors excised with half the tumor fixed for IHC and the other half frozen for molecular analyses.

In vivo *^{19}F MRS studies*

To confirm the efficacy of enzymatic conversion of 5-FC to 5-FU by yCD in the tumor, *in vivo* ^{19}F MRS was performed at the end of the final dose on a Bruker Biospec 9.4 T spectrometer as previously described [24]. Briefly, anesthetized mice were placed on an in-house constructed plastic cradle to allow positioning of the tumor in the RF coil. Following shimming on the water proton signal, serial nonselective ^{19}F MR spectra were acquired using a one-pulse sequence (flip angle, 60°; repetition time, 0.8 s; number of average, 2000; spectral width, 10 kHz; total acquisition time of 26 min). ^{19}F

MR spectra were processed with in-house XsOs nuclear magnetic resonance software developed by Dr. D. Shungu (Cornell University, New York, NY). The chemical shift of the 5-FU resonance was set to 0 ppm.

Immunohistochemistry

Formalin-fixed tumor tissues were embedded in paraffin and multiple 5 µm thick sections were cut. For each tumor, 2 adjacent sections were obtained from the largest cross-sectional tumor region with one section stained with H&E and the other immunostained for alpha smooth muscle actin (α-SMA). α-SMA IHC of tumor sections was performed using the streptavidin–peroxidase technique and the DAKO EnVision System (Dako Cytomation, Hamburg, Germany) following standard protocols as previously described [25].

High-resolution 20X digital scans of the H&E sections and the immunostained sections were obtained using ScanScope (Aperio, Vista, CA). Viable and necrotic regions were marked in the entire H&E section and mapped to the immunostained tissue section. The viable fraction was obtained by subtracting the necrotic region from the total region in the H&E section. For α-SMA IHC, the number of strongly positive pixels (NSP) was determined in the total tumor region, the entire viable region, and the entire necrotic region of each section using ImageScope software and algorithms supplied by the manufacturer (Aperio).

Molecular analyses

Freeze clamped tumor tissue was assayed for yCD, HIF-1α mRNA, and HIF-1 α protein expression. Briefly, snap-frozen PC3_HRE_LUC ($n=5$) and PC3_HRE_LUC_yCD ($n=5$) tumor samples were homogenized under liquid nitrogen. Powdered sample was weighed for RNA isolation and protein extraction. RNA was isolated following a standard protocol. Briefly, the tissue was first homogenized with RLT buffer and later passed through a QIAshredder and finally through an RNeasy mini kit column (Qiagen, Valencia, CA, USA) to obtain the RNA as per the manufacturer's instruction. cDNA was then synthesized using an iScript cDNA synthesis kit (Bio-Rad, Hercules, CA, USA). Quantitative real-time PCR was performed using Syber green (Bio-Rad) and gene specific primers. The expression of target RNA relative to the housekeeping gene hypoxanthine phosphoribosyltransferase 1 (HPRT1) was calculated based on the threshold cycle (Ct) as $R=2^{-\Delta(\Delta Ct)}$, where $\Delta Ct = Ct_{\text{target}} - Ct_{\text{HPRT1}}$ and $\Delta(\Delta Ct) = \Delta Ct_{\text{HRE\_LUC\_yCD}} - \Delta Ct_{\text{HRE\_LUC}}$.

For immunoblot analysis, protein was isolated from tumor tissue using RIPA (Radio Immuno Precipitation Assay) buffer after brief sonication following standard protocol. About 100 µg of total protein was resolved on a polyacrylamide gel (PAGE) and transferred to a nitrocellulose membrane overnight at 4 °C. The membrane was then probed for HIF-1α expression using antihuman HIF-1α monoclonal antibody (Cat. No. 610,958, Clone 52, BD Bioscience, San Jose, CA, USA). For loading control, anti-GAPDH antibody (SIGMA, St. Louis) was used to probe for GAPDH expression.

SHG microscopy

SHG microscopy of H&E stained sections was performed as previously described to evaluate Col1 fiber patterns [26]. Briefly, tiled scan SHG microscopy of the entire tissue section was performed to acquire Col1 fiber maps using an Olympus Laser Scanning FV1000 MPE multiphoton microscope (Olympus Corp., US headquarters–Center Valley, PA), with an incident laser wavelength of 860 nm and detection wavelength of 430 nm. A 25 × objective was used to acquire tiled scans. Tiled scans were acquired in X and Y directions to cover the entire tissue section, with a FOV of $425 \times 425\ \mu m^2$ per tile scan. Hot-spot regions with the highest Col1 fiber SHG signal intensity, identified based on the signal histogram for each tumor section, were analyzed for spatial distribution and texture patterns of Col1 fibers. Percent Col1 fiber volume and interfiber distance were computed from the Col1 SHG images using in-house software [27]. Texture analysis was performed to quantify Col1 fiber patterns using Haralick texture features from the gray level co-occurrence matrix (GLCM) [28] and Fourier transform texture analysis [29]. Several textural features were extracted by GLCM and Fourier transform texture analysis that reflect how the fibers are distributed with respect to each other. The GLCM extracted feature correlation is a measure of how a pixel is correlated to its neighboring pixel, with 1 for positively and −1 for negatively correlated pixels. Fourier transform texture features reflect the alignment of fiber distribution with respect to each other. For randomly distributed Col1 fibers, the resulting Fourier transform approximates a circle, whereas for fibers that are aligned parallel to each other in one direction, the Fourier transform is elliptical. The Fourier transform features were obtained by fitting an ellipse to the Fourier transform of each image. Fourier transform features included the aspect ratio (AR), which is the ratio of the major axis to the minor axis of the ellipse, and eccentricity, which is the ratio of the distance between the foci of the ellipse and the length of the major axis.

Statistical analysis

Statistical analysis was performed using an unpaired *t* test. *P* values ≤ 0.05 were considered significant unless otherwise stated.

Results

As shown in Figure 1C, bioluminescence was detected in genetically engineered PC3 cells stably expressing either HRE_LUC, or HRE_LUC_yCD following addition of luciferin in response to the hypoxia mimetic $CoCl_2$. Both PC3_HRE_LUC and PC3_HRE_LUC_yCD cells showed a statistically significant increase in luciferase activity in response to 24 h of hypoxia (Figure 1D). These data confirm the regulation of luciferase by hypoxia. An MTS assay was performed to further validate that HRE driven yCD converted the prodrug 5-FC to 5-FU in response to hypoxia. As shown in Figure 2, PC3_HRE_LUC cells did not show any decrease of cell viability in response to either hypoxia or to treatment with 1 mM 5-FC under normoxia or after hypoxic preconditioning of cells for 48 h (preconditioned cells). In contrast, 1 mM 5-FC treatment, following hypoxic preconditioning of PC3_HRE_LUC_yCD cells, resulted in a significant decrease of cell viability compared to all the groups. These data demonstrate the ability of the prodrug enzyme, expressed under hypoxic conditions, to form 5-FU from 5-FC and induce cell death.

Tumors derived from PC3 cells that expressed luciferase alone, or luciferase and yCD, under control of HRE were studied *in vivo* for their ability to report on hypoxia and selectively kill hypoxic cells. As shown in the representative images in Figure 3A, comparable regions of hypoxia were detected by BLI, in both PC3_HRE_LUC (left) and PC3_HRE_LUC_yCD tumors (right). The representative images in Figure 3B show that the hypoxic region decreased with 5-FC treatment in the PC3_HRE_LUC_yCD tumor (right) but not in the PC3_HRE_LUC tumor (left). Formation of yCD in the tumors was confirmed from analysis of yCD mRNA as shown in Figure 3C. Further confirmation of functional yCD was evident from the conversion of 5-FC to 5-FU as demonstrated in the spectra in Figure 3D acquired approximately 30 minutes after injection of 5-FC. The effects of the 5-FU formed from 5-FC resulted in a significant decrease of the volumes of PC3_HRE_LUC_yCD tumors compared to PC3_HRE_LUC tumors at 4 days after the third dose of 5-FC (Figure 3E).

Changes in bioluminescence confirmed the decrease of hypoxic cells in PC3_HRE_LUC_yCD tumors compared to PC3_HRE_LUC tumors. Data from 5 tumors per group are summarized in Figure 4A. There was no significant difference in the levels of pretreatment bioluminescence

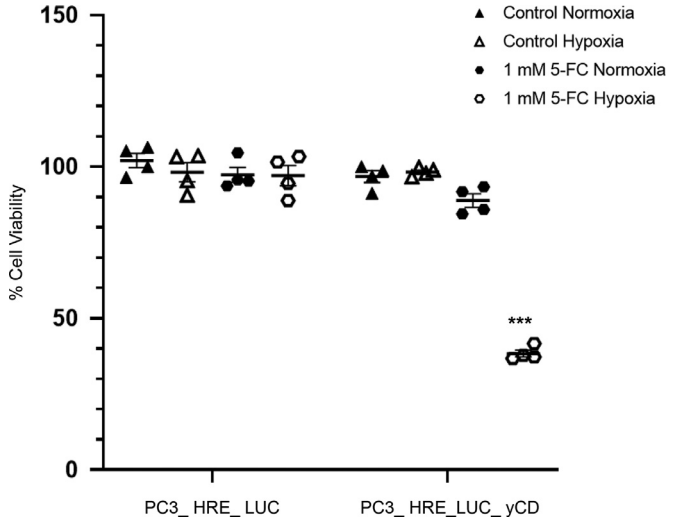

Figure 2. Cell viability, normalized to untreated wild type PC3 cells, following treatment with 1 mM of 5-fluorocytosine (5-FC) for 24 h in genetically engineered PC-3 cells that were maintained under normoxia or subject to 48 h of 1% O_2 before 5-FC treatment. Values represent Mean ± SEM of 4 independent experiments. Statistical analysis was performed using student's *t*-test. $^{***}P < 0.0005$ compared to all other groups.

between the 2 groups. Following 5-FC treatment, a significant decrease of bioluminescence was observed in PC3_HRE_LUC_yCD tumors (Figure 4A) within 3 days of the second 5-FC dose. A graph of bioluminescence *versus* tumor volume for PC3_HRE_LUC and PC3_HRE-LUC_yCD tumors presented in Figure 4B shows that hypoxia correlated with increasing tumor volumes in the PC3_HRE_LUC group ($r = 0.3506$, $P = 0.0429$). In the PC3_HRE_LUC_yCD group, although the correlation with tumor volume remained significant ($r = 0.4679$, $P = 0.0092$), tumors tended to be less hypoxic at comparable volumes. Analysis of HIF-1α mRNA confirmed the decrease of hypoxic cells in PC3_HRE_LUC_yCD tumors compared to PC3_HRE_LUC tumors following treatment (Figure 4C). Immunoblot analysis further identified a decrease of HIF-1α protein in 4 of the 5 PC3_HRE_LUC_yCD treated tumors compared to PC3_HRE_LUC tumors (Figure 4D).

As shown in the representative H&E sections in Figure 5A, 5-FC treatment resulted in a lower viable/necrotic fraction in PC3_HRE_LUC_yCD tumors (bottom) compared to PC3_HRE_LUC tumors (top). These data are summarized for 5 tumors from each group in Figure 5B and identify a trend toward a decrease of the viable to necrotic fraction in the tumors.

We analyzed the distribution of CAFs in the 2 tumor groups. Because CAFs infiltrate into necrotic regions, we analyzed the entire tumor section as well as the necrotic and viable areas. As shown in the representative examples from a PC3_HRE_LUC tumor (top) and a PC3_HRE_LUC_yCD tumor (bottom) in Figure 6A, α-SMA expression was heterogeneously distributed in tumor sections. However, the number of CAFs was lower in the PC3_HRE_LUC_yCD tumor compared to the PC3_HRE_LUC tumor. Quantification of the fraction of strongly positive pixels showed a statistically signification reduction of CAFs in the whole tumor and in the necrotic regions of PC3_HRE_LUC_yCD tumors compared to PC3_HRE_LUC tumors.

Representative SHG microscopy images from a PC3_HRE_LUC tumor (top) and a PC3_HRE_LUC_yCD tumor (bottom) are shown in Figure 7A. Data from the tumors are summarized in Figure 7B. Although the Col1 fiber content was not significantly different between the tumors, hot spot texture analysis of Col1 fibers (Figure 7B) detected significant differences between

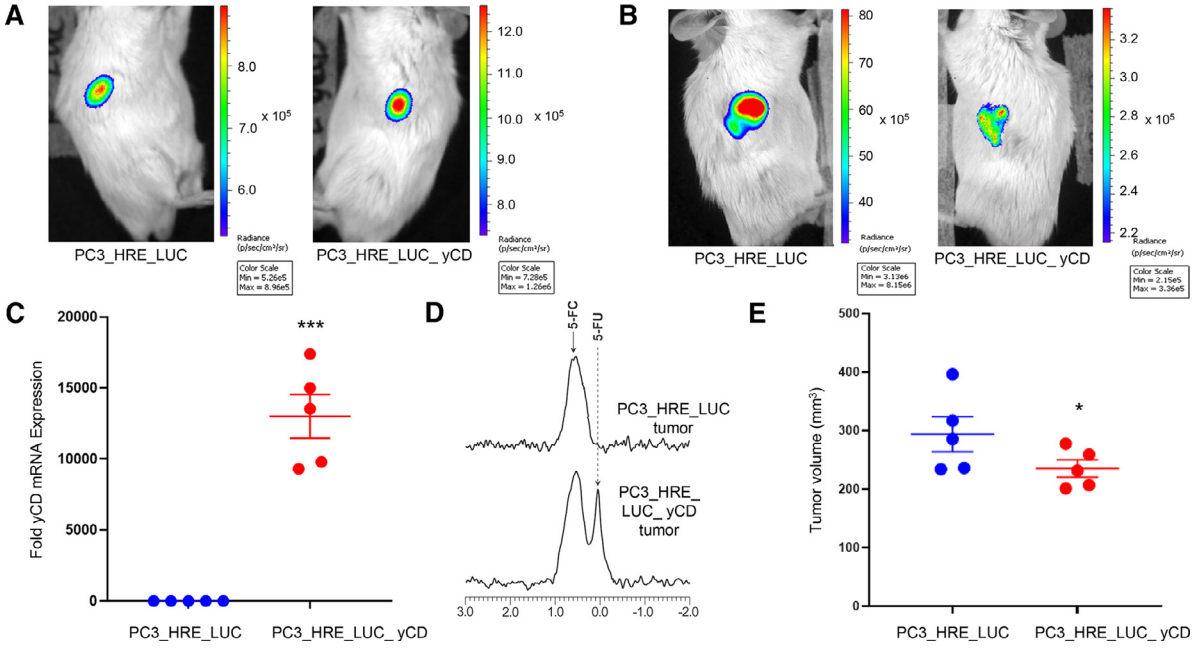

Figure 3. (A) Representative BL images of PC3_HRE_LUC (left) and PC3_HRE_LUC_yCD (right) tumors showing comparable hypoxic regions prior to treatment. (B) Representative BL images of PC3_HRE_LUC (left) and PC3_HRE_LUC_yCD (right) tumors showing a reduction of the hypoxic area only in the PC3_HRE_LUC_yCD tumor (right). (C) Fold change in yCD mRNA expression in PC3_HRE_LUC and PC3_HRE_LUC_yCD tumors. $^{***}P < 0.0005$. (D) Representative ^{19}F MR spectra obtained from a PC3_HRE_LUC tumor (top) and a PC3_HRE_LUC_yCD tumor (bottom) obtained ~30 minutes after injecting 5-FC. Arrow with dotted lines shows 5-FU peak. (E) Average tumor volume in mm^3 obtained 4 days after the third dose of 5-FC. Values represent Mean ± SEM of 5 tumors per group. $^{*}P < 0.05$.

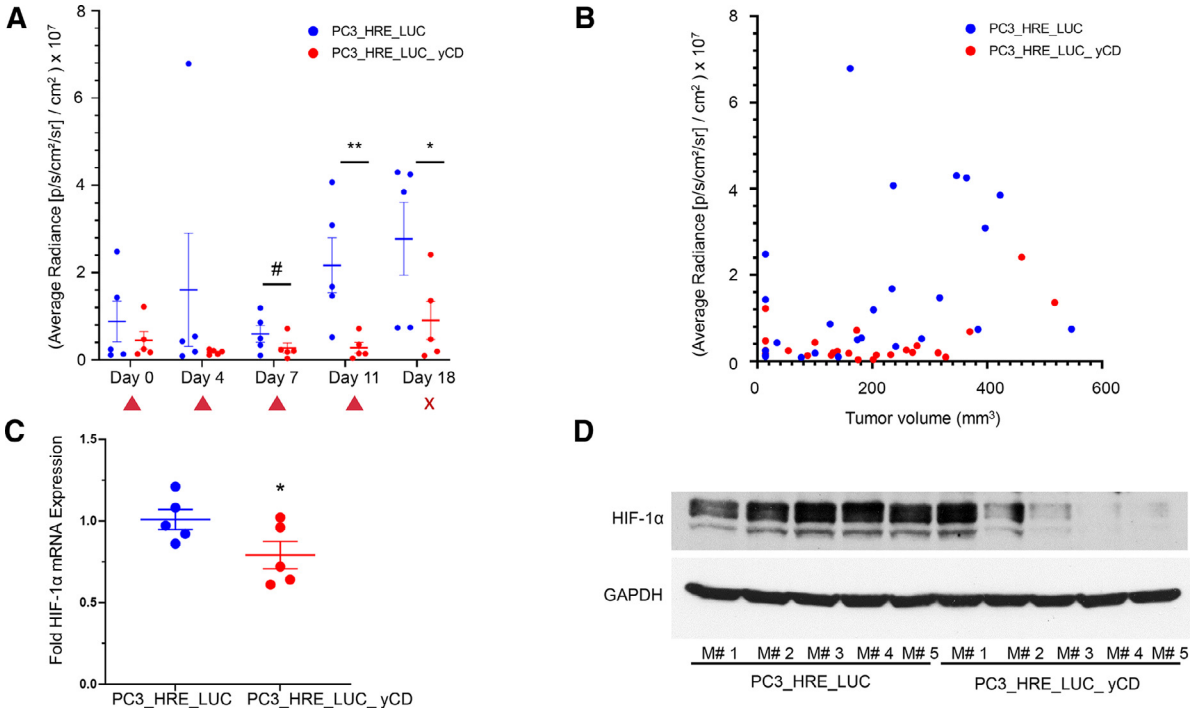

Figure 4. (A) Average radiance, obtained from the highest 40% BL intensity region normalized to the corresponding area, of PC3_HRE_LUC and PC3_HRE_LUC_yCD tumors during the course of the treatment. Values represent Mean ± SEM from 5 tumors per group. $\#P = 0.09$, $^{*}P < 0.05$, $^{**}P < 0.005$, PC3_HRE_LUC *vs* PC3_HRE_LUC_yCD. Symbols Δ and X on the X-axis represents day of 5-FC treatment and the day of sacrifice, respectively. BLI was performed immediately prior to 5-FC administration at each dose point. (B) Average radiance, obtained from the highest 40% BL intensity region normalized to the corresponding area, *vs* tumor volume for PC3_HRE_LUC and PC3_HRE-LUC_yCD tumors show that hypoxia correlated with increasing tumor volumes in the PC3_HRE_LUC group ($r = 0.3506$, $P = 0.0429$). In the PC3_HRE-LUC_yCD group, even at comparable volumes, these tumors tended to be less hypoxic although the correlation with tumor volume remained significant ($r = 0.4679$, $P = 0.0092$). (C) Fold change in HIF-1α mRNA expression in PC3_HRE_LUC and PC3_HRE_LUC_yCD tumors. $^{*}P < 0.05$. (D) Immunoblot of HIF-1α protein expression in PC3_HRE_LUC and PC3_HRE_LUC_yCD tumors.

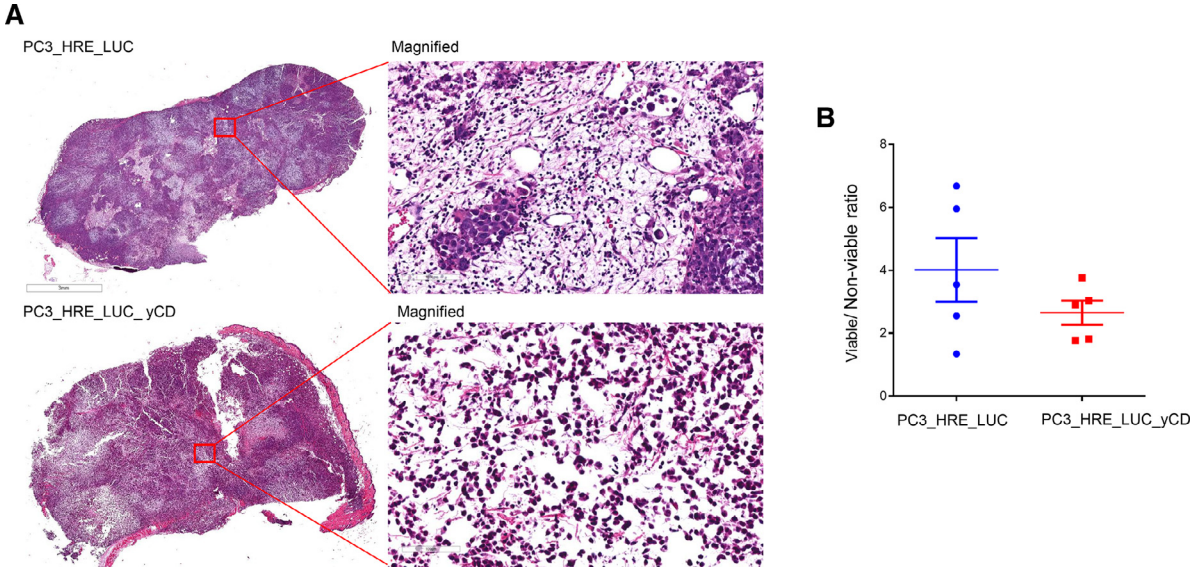

Figure 5. (A) Representative 1X H&E images of 5 µm thick sections from PC3_HRE_LUC (top) and PC3_HRE_LUC_yCD (bottom) tumors in response to 5-FC treatment. Corresponding magnified 20X H&E images from a region of interest are shown at the right. (B) Viable/Nonviable fraction obtained from tumors. Values represent Mean ± SEM from 5 tumors per group.

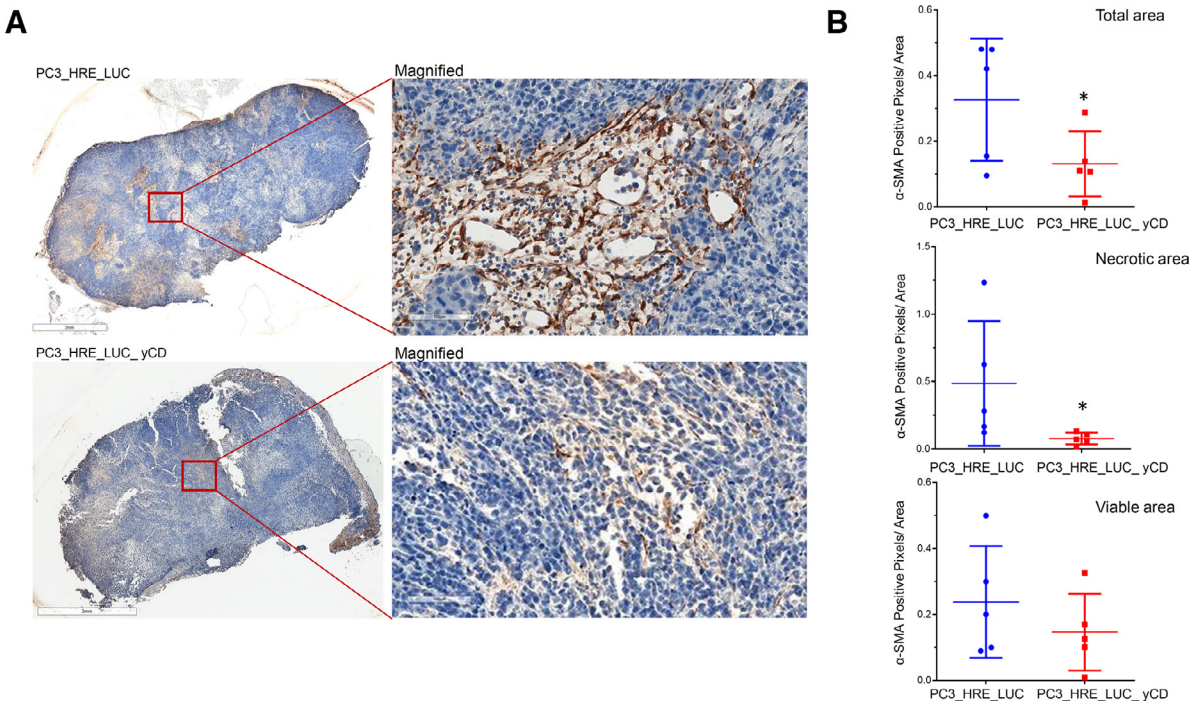

Figure 6. (A) Representative 1X α-SMA IHC images of 5 µm thick sections from PC3_HRE_LUC (top) and PC3_HRE_LUC_yCD (bottom) tumors in response to 5-FC treatment. Corresponding magnified 20X α-SMA IHC images from a region of interest are shown at the right. (B) Strongly positive pixel staining for α-SMA in the entire tumor (top), the necrotic fraction (middle), and the viable fraction (bottom) was quantified with ImageScope software using the positive pixel count algorithm supplied by manufacturer. Pixel intensity was normalized to the total number of pixels and expressed as percent strongly positive pixels. Values represent Mean ± SEM from 5 tumors per group. $^{*}P < 0.05$.

PC3_HRE_LUC and PC3_HRE_LUC_yCD tumors suggesting that the changes in CAFs in the PC3_HRE_LUC_yCD tumors did alter the Col1 fiber patterns in these tumors.

Discussion

Here we developed, for the first time, a theranostic imaging strategy that combined HRE driven expression of luciferase with HRE driven expression of a prodrug enzyme, yCD, to image and eliminate hypoxic cancer cell populations in tumors. With this strategy, we found a significant decrease of tumor volume, although the decrease of the viable/necrotic fraction was not significant. These data suggest that a combination of cell death and a decrease of cell proliferation likely contributed to the reduced tumor volume. Significant changes in the TME such as a significant reduction of CAFs, a decrease of HIF-1α, and changes in Col1 fiber patterns were identified. Based on the known roles of CAFs in increasing prostate cancer aggression [15], these data identify a decrease of the aggressive phenotype resulting from targeting hypoxic populations in these tumors.

In prostate cancer cell studies, HRE-driven bacterial CD transfected into androgen independent DU145 and androgen dependent 22Rv1 prostate cancer cell lines was used to sensitize hypoxic cells to radiation therapy and to 5-FU treatment [30]. CD is a nonmammalian enzyme found in bacteria and yeast that catalyzes the conversion of nontoxic 5-FC to the chemotherapeutic and radiosensitizing agent 5-FU [31]. 5-FU is an analog of uracil that is converted to several active metabolites such as fluorodeoxyuridine monophosphate (FdUMP), fluorodeoxyuridine triphosphate (FdUTP) and fluorouridine triphosphate (FUTP) that disrupt RNA synthesis as well as the action of the enzyme thymidylate synthase that is required for DNA synthesis [17]. In a previous study, we have demonstrated the feasibility of delivering bacterial CD with targeted or nontargeted nanoparticles (NPs) to tumors *in vivo* under image-guidance [24,32]. Image-guidance was used to time administration of 5-FC once the NPs were detected in the tumor and had cleared from normal tissue. We demonstrated successful conversion of 5-FC to 5-FU in tumors with ^{19}F MRS and a significant reduction of tumor growth [24,32]. Although bCD has higher stability [18] making it ideal for NP delivery approaches, yCD is significantly more active [19]. We therefore selected yCD for these studies. In earlier studies with HT29 [19] and U-87 cells [33] that expressed a yCD construct, 400–500 µM of 5-FC reduced the viability of cells exposed to 48 h of 0.1% O_2 by 90%. In our study 1 mM of 5-FC reduced cell viability by 65%. These differences in viability may be due to the differences in oxygen tension between the 2 studies and also due to variability in cell responses to 5-FU [34].

Our purpose here was to use this hypoxia theranostic approach to understand the impact of eliminating hypoxic cells on the TME, specifically CAFs. While the 5-FU produced by hypoxic cells in the tumor may have had a bystander effect on adjacent nonhypoxic cells, we clearly reduced hypoxic tumor populations as evident from the significant decrease of luciferase activity detected in the tumors with BLI, and the significant decrease of HIF-1α mRNA and protein.

In prostate cancer, CAFs have been shown to induce growth, confer castration-resistance, and increase metastatic potential [35]. We previously observed, in a human breast cancer xenograft, that acutely hypoxic tumor areas have increased CAFs [27]. However, the effects of eliminating hypoxic cancer cells on CAFs have not been previously investigated. Here we observed that eliminating hypoxic cancer cells resulted in a decrease of CAFs in the tumor, supporting the possibility that, in this prostate cancer xenograft, recruitment of CAFs was influenced by hypoxia dependent cytokines, resulting in a decrease of CAFs when hypoxic cancer cells were eliminated. In untreated tumors, hypoxic tumor regions evolve into necrotic regions explaining why CAFs are observed in hypoxic-necrotic regions. The decrease

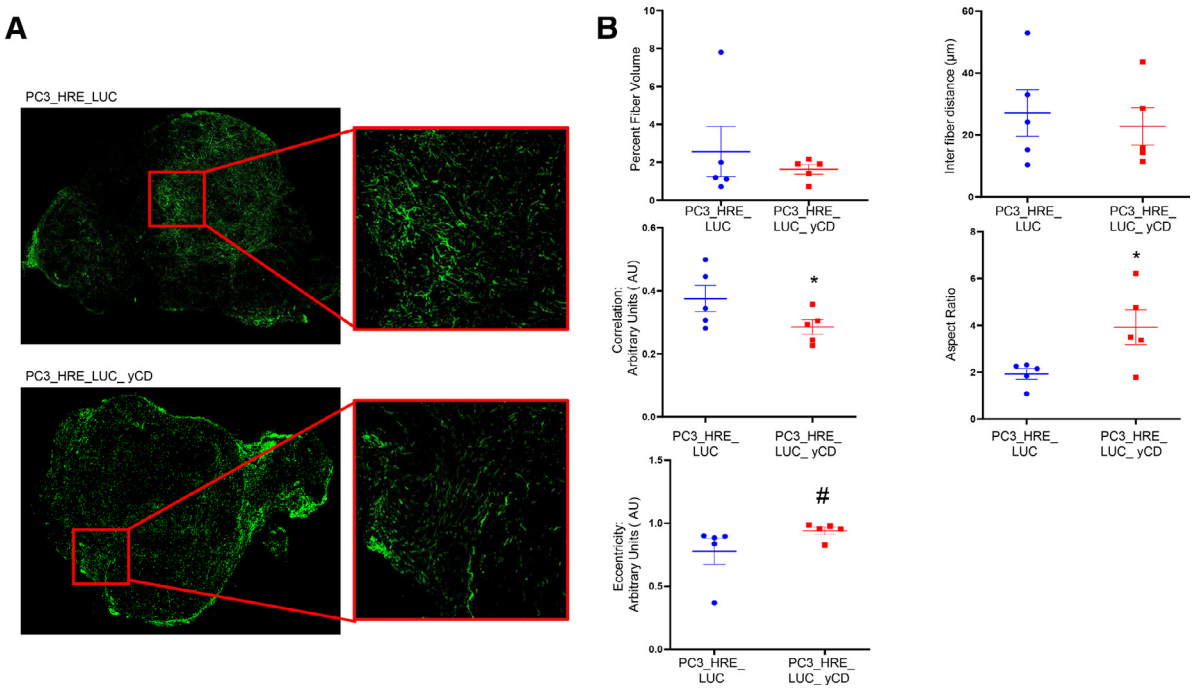

Figure 7. (A) Representative tile scanned Col1 fiber images acquired using SHG microscopy from a PC3_HRE_LUC (top) and PC3_HRE_LUC_yCD tumor (bottom) in response to 5-FC treatment. The images were acquired at a pixel resolution of 0.83 μm x 0.83 μm with a FOV of 425 × 425 μm^2 for each tile scan. Red boxes identify zoomed in regions for the 2 tumors. (B) Analysis from SHG microscopy showed no significant difference in percent fiber volume and interfiber distances between PC3_HRE_LUC tumors and the PC3_HRE_LUC_yCD tumors. However, differences in the texture patterns in the Col1 fiber distribution were observed between the PC3_HRE_LUC and the PC3_HRE_LUC_yCD tumors. The texture parameter correlation was significantly higher in the PC3_HRE_LUC tumors compared to the PC3_HRE_LUC_yCD tumors, the aspect ratio was significantly lower in PC3_HRE_LUC tumors compared to the PC3_HRE_LUC_yCD tumors, and eccentricity showed a trend toward lower values for the PC3_HRE_LUC tumors compared to the PC3_HRE_LUC_yCD tumors. Values represent Mean ± SEM. $^*P < 0.05$, # $P = 0.06$.

of the viable/necrotic fraction in the 5-FC treated PC3_HRE_LUC_yCD tumors was due to an increase of cell death from 5-FU and not from oxygen deprivation. It is possible that hypoxia results in the recruitment of CAFs, similar to wound-healing, where fibroblasts present in granulation tissue become myofibroblasts and deposit ECM components including mainly collagen type III that is gradually replaced by Col1 and elastin [13]. While we did not detect a significant change of Col1 fiber content, in the 5-FC treated PC3_HRE_LUC_yCD tumors, we did observe significant alterations in the Col1 fiber texture in these tumors. The impact of these alterations on tumor stiffness and on invasion and metastasis merit further investigation.

While we were able to demonstrate a reduction of tumor volume and hypoxia with our theranostic strategy, some of the constraints of our study were that the changes in CAFs were only evaluated 7 days after the end of treatment and not at intermediate time-points. We were therefore unable to identify the time at which CAF trafficking may have been altered. Additionally, although our data show that hypoxic cells were eliminated, the 5-FU generated may have also had a bystander effect on normoxic cells. HRE driven expression of BL only provided a hypoxia index and not oxygen tensions. Future studies should also investigate the effects of this hypoxia theranostic strategy on tumor metastasis.

In conclusion, here we have identified significant changes in the TME with a hypoxia theranostic strategy. These results expand our understanding of the effects of selectively eliminating hypoxic populations in tumors and support targeting hypoxia to decrease aggressive populations in tumors. Gene therapy was investigated in the treatment of human prostate cancer over a decade ago [36]. More recently, a Phase II/III clinical trial of patients with newly diagnosed glioblastoma injected with vocimagene amiretrorepvec (Toca 511), a replicative retrovirus (RRV) based therapeutic gene CD followed by extended release flucytosine (Toca FC) (TOCAGEN San Diego, CA, Clinical trials.gov, NRG-BN006), has also been performed. Selective elimination of hypoxic cancer cells may be possible in human cancers, in the future, with the development of targeted nanoparticles to deliver cDNA [37] of HRE controlled prodrug enzymes. Tailoring such RRVs to carry an HRE driven therapeutic gene may provide precision targeting of hypoxic cancer cells. There has been significant interest in developing hypoxia activated prodrugs (HAPs) [38]. Lessons learned from clinical trials of HAPs such as Evofosamide have clearly identified the importance of integrating hypoxia imaging with hypoxia targeting strategies [39–43]. Imaging of tumor targeted NPs delivering cDNA of a hypoxia driven prodrug enzyme in combination with hypoxia imaging using PET [44] or MRI [45] may provide translational approaches for hypoxia theranostics.

Author's contribution

BK and ZMB planned the study. BK, YM, FO, FW performed experiments. DJ, SB, LDS, MFP contributed to *in vivo* imaging. BK, ZMB, EG and SK performed data analysis. MEB provided the yCD construct. BK and ZMB wrote the manuscript. All authors edited the final manuscript.

Acknowledgments

This work was supported by NIH R35 CA209960, P41 EB024495, R01 CA253617, and R01 CA 82337. We thank Mr. Gary Cromwell for valuable technical assistance.

References

[1] Philip B, Ito K, Moreno-Sanchez R, Ralph SJ. HIF expression and the role of hypoxic microenvironments within primary tumours as protective sites driving cancer stem cell renewal and metastatic progression. *Carcinogenesis* 2013;**34**:1699–707.

[2] Ranasinghe WK, Baldwin GS, Shulkes A, Bolton D, Patel O. Normoxic regulation of HIF-1alpha in prostate cancer. *Nat Rev Urol* 2014;**11**:419.

[3] Miyazawa K, Tanaka T, Nakai D, Morita N, Suzuki K. Immunohistochemical expression of four different stem cell markers in prostate cancer: high expression of NANOG in conjunction with hypoxia-inducible factor-1alpha expression is involved in prostate epithelial malignancy. *Oncol Lett* 2014;**8**:985–92.

[4] Mathieu J, Zhang Z, Zhou W, Wang AJ, Heddleston JM, Pinna CM, Hubaud A, Stadler B, Choi M, Bar M, et al. HIF induces human embryonic stem cell markers in cancer cells. *Cancer Res* 2011;**71**:4640–52.

[5] Marhold M, Tomasich E, El-Gazzar A, Heller G, Spittler A, Horvat R, Krainer M, Horak P. HIF-1alpha regulates mTOR signaling and viability of prostate cancer stem cells. *Molecular Cancer Res* 2015;**13**:556–64.

[6] Ma Y, Liang D, Liu J, Axcrona K, Kvalheim G, Stokke T, Nesland JM, Suo Z. Prostate cancer cell lines under hypoxia exhibit greater stem-like properties. *PLoS One* 2011;**6**:e29170.

[7] Quail DF, Joyce JA. Microenvironmental regulation of tumor progression and metastasis. *Nat Med* 2013;**19**:1423–37.

[8] Josson S, Matsuoka Y, Chung LW, Zhau HE, Wang R. Tumor-stroma co-evolution in prostate cancer progression and metastasis. *Semin Cell Dev Biol* 2010;**21**:26–32.

[9] Kalluri R, Zeisberg M. Fibroblasts in cancer. *Nat Rev Cancer* 2006;**6**:392–401.

[10] Wen S, Niu Y, Yeh S, Chang C (2015). BM-MSCs promote prostate cancer progression via the conversion of normal fibroblasts to cancer-associated fibroblasts. Int J Oncol 47, 719–727.

[11] Barron DA, Rowley DR. The reactive stroma microenvironment and prostate cancer progression. *Endocr Relat Cancer* 2012;**19**:R187–204.

[12] Cirri P, Chiarugi P. Cancer associated fibroblasts: the dark side of the coin. *Am J Cancer Res* 2011;**1**:482–97.

[13] Franco OE, Hayward SW. Targeting the tumor stroma as a novel therapeutic approach for prostate cancer. *Adv Pharmacol* 2012;**65**:267–313.

[14] Byun JS, Gardner K. Wounds that will not heal: pervasive cellular reprogramming in cancer. *Am J Pathol* 2013;**182**:1055–64.

[15] Penet MF, Kakkad S, Pathak AP, Krishnamachary B, Mironchik Y, Raman V, Solaiyappan M, Bhujwalla ZM. Structure and function of a prostate cancer dissemination-permissive extracellular matrix. *Clin Cancer Res* 2017; **23**:2245–54.

[16] Raman V, Artemov D, Pathak AP, Winnard PT Jr, McNutt S, Yudina A, Bogdanov A Jr, Bhujwalla ZM. Characterizing vascular parameters in hypoxic regions: a combined magnetic resonance and optical imaging study of a human prostate cancer model. *Cancer Res.* 2006;**66**:9929–36.

[17] Longley DB, Harkin DP, Johnston PG. 5-fluorouracil: mechanisms of action and clinical strategies. *Nat Rev Cancer* 2003;**3**:330–8.

[18] Ireton GC, McDermott G, Black ME, Stoddard BL. The structure of *Escherichia coli* cytosine deaminase. *J Mol Biol* 2002;**315**:687–97.

[19] Kievit E, Bershad E, Ng E, Sethna P, Dev I, Lawrence TS, Rehemtulla A. Superiority of yeast over bacterial cytosine deaminase for enzyme/prodrug gene therapy in colon cancer xenografts. *Cancer Res.* 1999;**59**:1417–21.

[20] Harada H, Kizaka-Kondoh S, Itasaka S, Shibuya K, Morinibu A, Shinomiya K, Hiraoka M. The combination of hypoxia-response enhancers and an oxygen-dependent proteolytic motif enables real-time imaging of absolute HIF-1 activity in tumor xenografts. *Biochem Biophys Res Commun* 2007;**360**:791–6.

[21] Stolworthy TS, Korkegian AM, Willmon CL, Ardiani A, Cundiff J, Stoddard BL, Black ME. Yeast cytosine deaminase mutants with increased thermostability impart sensitivity to 5-fluorocytosine. *J Mol Biol* 2008;**377**:854–69.

[22] Danhier P, Krishnamachary B, Bharti S, Kakkad S, Mironchik Y, Bhujwalla ZM. Combining optical reporter proteins with different half-lives to detect temporal evolution of hypoxia and reoxygenation in tumors. *Neoplasia* 2015;**17**:871–81.

[23] Bharti SK, Kakkad S, Danhier P, Wildes F, Penet MF, Krishnamachary B, Bhujwalla ZM. Hypoxia patterns in primary and metastatic prostate cancer environments. *Neoplasia* 2019;**21**:239–46.

[24] Li C, Penet MF, Wildes F, Takagi T, Chen Z, Winnard PT, Artemov D, Bhujwalla ZM. Nanoplex delivery of siRNA and prodrug enzyme for multimodality image-guided molecular pathway targeted cancer therapy. *ACS Nano* 2010;**4**:6707–16.

[25] Heo SC, Lee KO, Shin SH, Kwon YW, Kim YM, Lee CH, Kim YD, Lee MK, Yoon MS, Kim JH. Periostin mediates human adipose tissue-derived mesenchymal stem cell-stimulated tumor growth in a xenograft lung adenocarcinoma model. *Biochim Biophys Acta* 2011;**1813**:2061–70.

[26] Kakkad S, Zhang J, Akhbardeh A, Jacob D, Krishnamachary B, Solaiyappan M, Jacobs MA, Raman V, Leibfritz D, Glunde K, et al. Collagen fibers mediate MRI-detected water diffusion and anisotropy in breast cancers. *Neoplasia* 2016;**18**:585–93.

[27] Kakkad SM, Solaiyappan M, O'Rourke B, Stasinopoulos I, Ackerstaff E, Raman V, Bhujwalla ZM, Glunde K. Hypoxic tumor microenvironments reduce collagen I fiber density. *Neoplasia* 2010;**12**:608–17.

[28] Haralick RM, Dinstein I, Shanmugam K. Textural Features for Image Classification. IEEE Transactions on Systems, Man and Cybernetics; 1973. p. 610–21. **SMC-3**.

[29] Kakkad SM, Solaiyappan M, Argani P, Sukumar S, Jacobs LK, Leibfritz D, Bhujwalla ZM, Glunde K. Collagen I fiber density increases in lymph node positive breast cancers: pilot study. *J Biomed Opt* 2012;**17**:116017.

[30] Marignol L, Foley R, Southgate TD, Coffey M, Hollywood D, Lawler M. Hypoxia response element-driven cytosine deaminase/5-fluorocytosine gene therapy system: a highly effective approach to overcome the dynamics of tumour hypoxia and enhance the radiosensitivity of prostate cancer cells *in vitro*. *J Gene Med* 2009;**11**:169–79.

[31] Heidelberger C, Danenberg PV, Moran RG. Fluorinated pyrimidines and their nucleosides. *Adv Enzymol Relat Areas Mol Biol* 1983;**54**:58–119.

[32] Chen Z, Penet MF, Nimmagadda S, Li C, Banerjee SR, Winnard PT Jr, Artemov D, Glunde K, Pomper MG, Bhujwalla ZM. PSMA-targeted theranostic nanoplex for prostate cancer therapy. *ACS Nano* 2012;**6**:7752–62.

[33] Wang D, Ruan H, Hu L, Lamborn KR, Kong EL, Rehemtulla A, Deen DF. Development of a hypoxia-inducible cytosine deaminase expression vector for gene-directed prodrug cancer therapy. *Cancer Gene Ther* 2005;**12**:276–283.

[34] Liu J, Harada H, Ogura M, Shibata T, Hiraoka M. Adenovirus-mediated hypoxia-targeting cytosine deaminase gene therapy enhances radiotherapy in tumour xenografts. *Br J Cancer* 2007;**96**:1871–8.

[35] Thalmann GN, Rhee H, Sikes RA, Pathak S, Multani A, Zhau HE, Marshall FF, Chung LW. Human prostate fibroblasts induce growth and confer castration resistance and metastatic potential in LNCaP Cells. *Eur Urol* 2010;**58**:162–171.

[36] Freytag SO, Khil M, Stricker H, Peabody J, Menon M, DePeralta-Venturina M, Nafziger D, Pegg J, Paielli D, Brown S, et al. Phase I study of replication-competent adenovirus-mediated double suicide gene therapy for the treatment of locally recurrent prostate cancer.. *Cancer Res.* 2002;**62**:4968–76.

[37] Chen Z, Penet MF, Krishnamachary B, Banerjee SR, Pomper MG, Bhujwalla ZM. PSMA-specific theranostic nanoplex for combination of TRAIL gene and 5-FC prodrug therapy of prostate cancer. *Biomaterials* 2016;**80**:57–67.

[38] Phillips RM. Targeting the hypoxic fraction of tumours using hypoxia-activated prodrugs. *Cancer Chemother Pharmacol* 2016;**77**:441–57.

[39] Borad MJ, Reddy SG, Bahary N, Uronis HE, Sigal D, Cohn AL, Schelman WR, Jr JS, Chiorean EG, Rosen PJ, et al. Randomized phase II trial of gemcitabine plus TH-302 versus gemcitabine in patients with advanced pancreatic cancer. *J Clin Oncol* 2015;**33**:1475–81.

[40] Chawla SP, Cranmer LD, Van Tine BA, Reed DR, Okuno SH, Butrynski JE, Adkins DR, Hendifar AE, Kroll S, Ganjoo KN. Phase II study of the safety and antitumor activity of the hypoxia-activated prodrug TH-302 in combination with doxorubicin in patients with advanced soft tissue sarcoma. *J Clin Oncol* 2014;**32**:3299–306.

[41] Peeters SG, Zegers CM, Biemans R, Lieuwes NG, van Stiphout RG, Yaromina A, Sun JD, Hart CP, Windhorst AD, van Elmpt W, et al. TH-302 in combination with radiotherapy enhances the therapeutic outcome and is associated with pretreatment [18F]HX4 hypoxia PET imaging. *Clin Cancer Res* 2015;**21**:2984–92.

[42] Spiegelberg L, Houben R, Niemans R, de Ruysscher D, Yaromina A, Theys J, Guise CP, Smaill JB, Patterson AV, Lambin P, et al. Hypoxia-activated prodrugs and (lack of) clinical progress: the need for hypoxia-based biomarker patient selection in phase III clinical trials.. *Clin Transl Radiat Oncol* 2019;**15**:62–9.

[43] Weiss GJ, Infante JR, Chiorean EG, Borad MJ, Bendell JC, Molina JR, Tibes R, Ramanathan RK, Lewandowski K, Jones SF, et al. Phase 1 study of the safety, tolerability, and pharmacokinetics of TH-302, a hypoxia-activated prodrug, in patients with advanced solid malignancies. *Clin Cancer Res* 2011;**17**:2997–3004.

[44] Yamamoto Y, Maeda Y, Kawai N, Kudomi N, Aga F, Ono Y, Nishiyama Y. Hypoxia assessed by 18F-fluoromisonidazole positron emission tomography in newly diagnosed gliomas. *Nucl Med Commun* 2012;**33**:621–5.

[45] Salem A, Little RA, Latif A, Featherstone AK, Babur M, Peset I, Cheung S, Watson Y, Tessyman V, Mistry H, et al. Oxygen-enhanced MRI is feasible, repeatable, and detects radiotherapy-induced change in hypoxia in xenograft models and in patients with non-small cell lung cancer. *Clin Cancer Res* 2019;**25**:3818–29.